CORROSION
The Journal of Science and Engineering

# Characterization of the Corrosion Product Films Formed on the As-cast and Friction-stir Processed Ni–Al Bronze in a 3.5 wt.% NaCl Solution



| | |
|---|---|
| Journal: | *Corrosion* |
| Manuscript ID: | CJ-1406-OA-1391.R2 |
| Manuscript Type: | Original Article |
| Date Submitted by the Author: | 28-Oct-2014 |
| Complete List of Authors: | ZHENG, Yugui; INST. OF METAL RESEARCH, CAS, Key Laboratory of Nuclear Materials and Safety Assessment,<br>Song, Qining; INST. OF METAL RESEARCH, CAS,, State Key Laboratory for Corrosion and Protection<br>Ni, D.R.; INST. OF METAL RESEARCH, CAS,<br>Ma, Z.Y.; INST. OF METAL RESEARCH, CAS,, State Key Laboratory for Corrosion and Protection |
| Key Words: | artificial seawater, erosion-corrosion, film |
| | |

# Characterization of the Corrosion Product Films Formed on the As-cast and Friction-stir Processed Ni–Al Bronze in a 3.5 wt.% NaCl Solution

**Q.N. Song [a], Y.G. Zheng [a,*], D.R. Ni [b], Z.Y. Ma [b]**

[a] Key Laboratory of Nuclear Materials and Safety Assessment, Institute of Metal Research, Chinese Academy of Sciences, 62 Wencui Road, Shenyang 110016, China

[b] Shenyang National Laboratory for Materials Science, Institute of Metal Research, Chinese Academy of Sciences, 72 Wenhua Road, Shenyang 110016, China



*Corresponding author.
Tel: +86 24 23928381; fax: +86 24 23894149
E-mail: ygzheng@imr.ac.cn

## ABSTRACT

An as-cast Ni–Al bronze (NAB) was subjected to friction-stir processing (FSP). The friction-stir processed NAB (FSPed NAB) exhibited better corrosion resistance in a 3.5 wt.% sodium chloride solution. The corrosion product films formed on the as-cast and FSPed NAB were characterized by scanning electron microscopy (SEM), X-Ray diffraction (XRD) and electron probe micro-analysis (EPMA). Uncorroded phases were retained in the films. The interfaces between these phases and their surrounding corrosion products would allow the chloride ions in and reduce the film protectiveness. For the as-cast NAB, the uncorroded phases were large in size or continuous in structure, resulting in continuous interfaces. Therefore, the film on the as-cast NAB exhibited relatively inferior protectiveness. The films on the as-cast and FSPed NAB were similar in composition, with mainly copper chloride hydroxide $Cu_2(OH)_3Cl$ in the outer layer, and $Al_2O_3$ and $Cu_2O$ with the incorporation of Fe and Ni in the inner layer. Stability of the films in the flowing condition was also studied and a film damage mechanism was raised. In the flowing condition, the film on the as-cast NAB was damaged by crack formation and expansion, while the film on the FSPed NAB was damaged by thinning.


**Keywords:** Ni–Al bronze; Friction-stir processing; Corrosion product film; SEM; EPMA; XRD; Flowing condition.

## INTRODUCTION

Due to the high strength, fracture toughness and corrosion/cavitation erosion resistance, Ni–Al bronze (NAB) has been widely used for marine components, including ship propellers, pumps and valves, etc. [1-3] NAB is a quaternary alloy with the addition of 9–12 wt.% Al and 6 wt.% each of Ni and Fe. The excellent corrosion resistance of NAB in chloride-containing media is attributed to a protective corrosion product film. [2–6] The corrosion product film on NAB has been investigated in many research works. [3–6] It was reported that the film consisted of two layers, with $Cu_2O$ in the outer layer and $Al_2O_3$ in the inner layer. [4] The protective film of copper alloys continued to improve in the stagnant and flowing seawater and maintained at a steady state, provided that the flow velocity did not exceed a specific threshold value; [5] whereas, damage occurred to the film of NAB in the flowing media of high flow velocities or of high degree of turbulence. [6] However, the direct morphology or structure of the corrosion product film on NAB has been rarely exhibited, probably due to the fact that the film is very thin, i.e., about 800 nm as reported. [4]

The ship propellers made of NAB are often large castings. The casting porosities and the inhomogeneous and coarse cast microstructure reduce the lifetime of the propellers. These casting defects make the corrosion product film formed on NAB discontinuous and inhomogeneous, and consequently reduce the film protectiveness. In order to overcome these casting defects, friction-stir processing (FSP) which is a solid-state processing method, was applied to the cast NAB in our previous study. [7]

FSP is originated from friction-stir welding (FSW).[8] It is operated below the melting point of the materials. During FSP, a non-consumable rotating tool inserts into a component and then traverses along the preferred path to modify the microstructure. It was reported that FSP homogenized and refined the cast microstructure, eliminated the casting porosities, and consequently improved the mechanical properties and corrosion resistance of the cast Al-, Ti-, Cu-based alloys, etc.[9–15] Our previous study showed that the friction-stir processed NAB (stated as FSPed NAB hereinafter) exhibited better corrosion resistance than the as-cast NAB in a 3.5 wt.% sodium chloride (NaCl) solution, and a more protective film formed on it.[14] However the corrosion product films formed on the as-cast and FSPed NAB have not been further characterized.

In this study, the corrosion product films formed on the as-cast and FSPed NAB after immersion in a stagnant 3.5 wt.% NaCl solution for 60 days were characterized and compared with each other. The morphologies of the corrosion product films were observed by scanning electron microscopy (SEM). The compositions of the corrosion product films were characterized by X-Ray diffraction (XRD) and electron probe micro-analysis (EPMA). Electrochemical measurements were carried out to study the stability of the corrosion product films in the flowing medium.

## EXPERIMENTAL

### Materials

An as-cast UNS C95800 NAB (chemical composition in wt.%: Al, 9.18; Ni, 4.49;

Fe, 4.06; Mn, 1.03 and Cu balance) plate with dimensions of 300 mm × 70 mm × 8 mm was subjected to FSP, as shown in Figure 1(a). A nickel-based alloy tool comprising a concave shoulder with a diameter of 24 mm, and a threaded conical pin with a root diameter of 8 mm and a length of 7 mm was used. The rotating rate and traverse speed of the processing tool were 1200 rpm and 50 mm/min, respectively. The cross section morphology of the plate was shown in Figure 1(b). The microstructures of the as-cast and FSPed NAB were observed with an optical microscope after etching with a solution containing 5 g of iron(III) chloride ($FeCl_3$), 2 mL of hydrochloric acid (HCl) and 95 mL of ethanol ($C_2H_5OH$).

**Characterization of the corrosion product films**

The gravimetric measurements were performed on the as-cast and FSPed NAB samples with dimensions of 14 mm × 10 mm × 2 mm. The sampling position for the FSPed NAB was in the center of the stirred zone, as shown in Figure 1(c). A minimum of three samples were prepared for both the as-cast and FSPed NAB in order to ensure accuracy. Each of the samples was successively ground with abrasive papers up to 1000 grit, ultrasonically cleaned in ethanol, dried with blowing air and weighed as $m_1$. It was then immersed in a container filled with 1.5 L of an aerated 3.5 wt.% NaCl solution (made of the analytical-grade reagent and distilled water). The solution was replaced every week to keep fresh. After immersion for 60 days, the sample was taken out, rinsed with distilled water, dried and weighed as $m_2$. Subsequently, it was immersed in a solution containing 500 mL of HCl and 500 mL of distilled water for two minutes to remove the corrosion products, and weighed as $m_3$

after ultrasonically cleaning and drying. The weight loss of a fresh sample after immersion in this solution for two minutes was less than 0.1 mg. Therefore, the solution caused little weight loss of the substrate beneath the corrosion products. The weight loss of the sample and the weight of the corrosion products were noted as $m_1$–$m_3$ and $m_2$–$m_3$, respectively.

The surface and cross section morphologies of the corroded as-cast and FSPed NAB were observed by SEM (FEI-Inspect F, acceleration voltage 25 kV). EPMA (Shimadzu, 1610) was used to analyze the element distribution of the corrosion product films. In order to minimize the effect of high peak intensities from the substrate, grazing incidence XRD analysis was conducted on the corrosion product films using an X-ray diffractometer (X'Pert PRD, PANalytical, Holland) with Cu Kα radiation, the diffraction angle range was 10–85° and the incidence angle was 0.6°.

**Electrochemical measurements in the flowing condition**

A modified rotating disk rig was used in this study to simulate the flowing condition. Its schematic diagram was shown in Figure 2. The tested sample was fixed on the disc and the container was filled with the testing medium. When the disc rotated, the medium flowed at a specific velocity relative to the sample. The velocity of the flowing medium was derived from the rotating rate of the disk and the distance from the sample to the center of the disk.

Each of the as-cast and FSPed NAB samples was firstly mounted in a plastic tube by a two-component epoxy resin, with a Cu wire welded at the back and leaving an area of 0.49 $cm^2$ exposed; then it was immersed in the stagnant 3.5 wt.% NaCl

solution for a duration of 60 days. The sample after the immersion was termed as the filmed as-cast or FSPed NAB hereinafter. The electrochemical measurements were conducted in a typical three-electrode system. The working electrode was the filmed as-cast or FSPed NAB. Two graphite rods and a saturated calomel electrode (SCE) served as the counter and reference electrode, respectively. The test medium was 5.5 L of a 3.5 wt.% NaCl solution with the addition of 1 wt.% dried silica sand. The average size of the sand was about 150 μm in diameter. The pH value of the 3.5 wt.% NaCl solution changed little after the addition of the silica sand. The velocity of the flowing medium was 4 m/s and the Reynolds number was about $2.6\times10^5$, indicating that the present flowing condition was in a state of turbulence. The electrochemical impedance spectrum (EIS) tests were carried out from 100 kHz to 10 mHz with a 5 mV perturbation using Gamry Interface 1000 to monitor the surface change of the filmed as-cast and FSPed NAB. A minimum of three samples were tested to ensure reproducibility for both the as-cast and FSPed NAB.

## RESULTS AND DISCUSSION

### Microstructure analysis

Figure 3 shows the microstructures of the as-cast and FSPed NAB. The as-cast NAB is composed of higher than 100-μm coarse Widmanstätten α phases, $\kappa_{II}$ , lamellar eutectoid α + $\kappa_{III}$, $\kappa_{IV}$ and some β' phases (transformation products of the high temperature β phase), as indicated in Figure 3(a). $\kappa_{II}$ is mainly distributed at the phase boundaries with a size of 1–3 μm and $\kappa_{IV}$ is a precipitate within the α phase with a size of lower than 1 μm. The stirred zone in the FSPed NAB consists of four

different microstructures along the plate thickness, namely Widmanstäten α and β' phases, banded α and β', equiaxed α and β' and stream-like α and β'.[7] The equiaxed microstructure in the center of the stirred zone is demonstrated in Figure 3(b), the lightly etched α is about 10 μm.

**Structures of the corrosion product films**

Figure 4 shows the weight loss and the weight of the corrosion product film for the as-cast and FSPed NAB after immersion in the 3.5 wt.% NaCl solution for 60 days. The weight loss of the FSPed NAB is much lower than that of the as-cast NAB, indicating that the corrosion product film on the FSPed NAB is more protective. This is consistent with our previous study.[12, 14] The weight of the corrosion product film is larger for the as-cast NAB. This finding demonstrates that a much thicker corrosion product film is formed on the as-cast NAB. However, the film is less protective probably due to its loose and inhomogeneous structure.

A loose needle-shaped corrosion product is found on the surfaces of the as-cast and FSPed NAB, as exhibited in Figure 5 after immersion in the 3.5 wt.% NaCl solution for 60 days. It is more enriched on the as-cast NAB. For the as-cast NAB, it mainly locates over the lamellar eutectoid; whereas for the FSPed NAB, it mainly locates over the β' phases as indicated by arrows.

Figure 6 shows the back-scattered electron (BSE) images of the as-cast and FSPed NAB in the cross section after immersion in the 3.5 wt.% NaCl solution for 60 days. For the as-cast NAB, the corrosion product films formed on various phases are different with each other, as shown in Figure 6(a). The corrosion product film is

thinner on the α phase, i.e., less than 1 μm, as indicated in Figure 6(c). It is thicker on the lamellar α + $\kappa_{III}$, i.e., more than 7 μm, as indicated in Figure 6(b). Moreover, it is noted that the κ phases are uncorroded and retained in the corrosion product film. In the cast microstructure, $\kappa_{IV}$ and $\kappa_{II}$ were based on $Fe_3Al$ and the lamellar $\kappa_{III}$ was based on NiAl.[16] According to Wharton,[3] the κ phases were protected in nearly neutral chloride media because they were Al-abundant and a protective $Al_2O_3$ film formed on them. Therefore, it was the α matrix and the lamellar α that suffered preferential corrosion,[17,18] resulting in the retention of the κ phases in the corrosion product film. Compared to the α matrix, the lamellar α was more severely corroded because the anode (i.e., the lamellar α) and cathode (i.e., $\kappa_{III}$) were alternately distributed in the lamellar eutectoid. As demonstrated in Figure 6(b), the corrosion pit at the lamellar eutectoid is about 7 μm deeper than that at the α matrix.

For the FSPed NAB, β' is severely corroded as indicated in Figure 6(d). The corrosion pit at the β' phase is about 2 μm deeper than that at the α phase, as shown in Figure 6(e). The small-sized phases inside β' are uncorroded and retained in the corrosion product film. β', also termed as the retained β phase, was the transformation product of the high-temperature β phase under conditions of rapid cooling. β' was preferentially attacked in seawater.[18] During the heating process of FSP, $\kappa_{II}$ and $\kappa_{III}$ were not completely dissolved into β because the temperature was either not sufficiently high enough or of a sufficient duration. They were refined and spheroidized by the severe deformation during FSP.[13] The small-sized phases inside β' were the refined κ phases. Therefore, they were protected because of the formation of

a protective $Al_2O_3$ film in the 3.5 wt.% NaCl solution. It was the surrounding β' phase that was preferentially corroded and the small-sized phases were retained in the corrosion product film.

For the as-cast and FSPed NAB, these uncorroded phases were detrimental to the protectiveness of the corrosion product films. The interfaces between these uncorroded phases and their surrounding corrosion products (metallic oxides or chlorides) would be the most susceptible sites to allow the corrosive medium in, resulting in further corrosion of the substrate beneath the corrosion product film. These uncorroded phases also increased the growth stress inside the film and consequently raised the risk of the crack growth. For the as-cast NAB, the uncorroded lamellar $\kappa_{III}$ and large-sized $\kappa_{II}$ were even partly in the corrosion product film and partly in the substrate, as shown in Figure 6(c). This would provide direct paths for the chloride ion to penetrate into the substrate and cause further corrosion. However, due to the heat input and severe concurrent deformation during FSP, the cast microstructure was refined and homogenized. Therefore, the corrosion product film formed on the FSPed NAB was more homogeneous than that on the as-cast NAB. The uncorroded small-sized phases inside β' in the corrosion product film on the FSPed NAB were randomly distributed; thus, the growth stress inside the film was effectively dispersed. Moreover, the interfaces between the uncorroded phases and their surrounding corrosion products in the film were discontinuous; consequently it was difficult for the chloride ions to penetrate into the film or even the substrate. Therefore, the corrosion product film on the FSPed NAB was more protective.

The corrosion product films of the as-cast and FSPed NAB consist of two layers, with the outer layer in a discontinuous distribution, as shown in Figures 6(b) and (f), respectively. For the as-cast NAB, the outer layer is mainly located over the lamellar α + $\kappa_{III}$; whereas for the FSPed NAB, it is mainly located over the β' phases. Moreover, this layer is more enriched for the as-cast NAB. The outer layer was non-protective to the substrate because it was discontinuous. It corresponded to the needle-shaped corrosion product exhibited in Figure 5.

**Compositions of the corrosion product films**

The XRD patterns of the corrosion product films are shown in Figure 7. The copper chloride hydroxide, probably $Cu_2(OH)_3Cl$, is identified in the corrosion product films on the as-cast and FSPed NAB. However, other probable corrosion products, including $Cu_2O$, are not detected probably because they are in a small amount or of an amorphous structure.[4] Figure 8 shows the element mapping of the corrosion product films. The inner layer mainly contains the metallic oxides or hydroxides, because it is abundant in O and rare in Cl. Fe and Ni are more abundant in the inner layer than in the substrate. In contrast, the outer layer is abundant in Cu, Cl and O, and rare in Ni, Fe and Al.

It was generally accepted that for copper and its alloys in seawater, $Cu_2O$ was formed through the anodic reaction:

$$Cu \rightarrow Cu^{+} + e^{-}, \quad (1)$$

followed by the formation and the subsequent hydrolysis of the dichlorocuprous anions:[19–21]

$$Cu^{+} + 2Cl^{-} \rightarrow CuCl_2^{-}, \quad (2)$$

$$2CuCl_2^{-} + H_2O \rightarrow Cu_2O + 4Cl^{-} + 2H^{+}. \quad (3)$$

The $Cu_2O$ film is a p-type semiconductor with a defective structure, it can accept the foreign ions, such as Ni and Fe ions, to incorporate into the cation vacancies inside, hence the film protectiveness is further improved.[22–24] Based on the previous research works[4,22–26] and the present EPMA results indicated in Figure 8, $Cu_2O$ was probably the main corrosion product in the inner layer of the film for both the as-cast and FSPed NAB. Fe and Ni were incorporated into the lattice of $Cu_2O$ and therefore, they were enriched in the inner layer. It was reported that the corrosion product films of a duplex nature, with $Cu_2O$ in the outer layer and $Al_2O_3$ in the inner layer were formed on NAB[4] and a ternary Cu–Al–Ni alloy.[25–26] $Al_2O_3$ was formed with the dissolution of Al through the following process:[26]

$$Al + 4Cl^{-} \rightarrow AlCl_4^{-} + 3e^{-}, \quad (4)$$

$$AlCl_4^{-} + 2H_2O \rightarrow Al_2O_3 + 4Cl^{-} + 3H^{+}. \quad (5)$$

However, the EPMA results demonstrated that Al was distributed evenly in the inner layers of the corrosion product films in this study. It was reported that Al had a greater affinity for oxygen than Cu, and $Al_2O_3$ was more stable than $Cu_2O$.[3] For the Al bronzes, with the dissolution of Cu, the limiting mole fraction for aluminum oxide formation $N_{Al_2O_3}$ was achieved and then $Al_2O_3$ was formed on the surface.[27] However, the microstructures of the as-cast and FSPed NAB were complex, resulting in different Cu dissolution rates at various phases; hence, $Al_2O_3$ could not be formed simultaneously on different phases. The discontinuous $Al_2O_3$ layer on the surface was

not that impermeable to the passage of cuprous cations. Therefore, the inner layer of the corrosion product film consisted of a mixed $Al_2O_3$ and $Cu_2O$ with the incorporation of Fe and Ni. After long-term immersion in seawater, copper chloride hydroxides, including $Cu_2(OH)_3Cl$ and Cu(OH)Cl, formed on the copper alloys.[19–22] The following reaction led to the formation of $Cu_2(OH)_3Cl$: [20–22]

$$Cu_2O + Cl^- + 2H_2O \rightarrow Cu_2(OH)_3Cl + H^+ + 2e^- \quad (6)$$

In this study, $Cu_2(OH)_3Cl$ was also detected by XRD. It was mainly located in the outer layers of the corrosion product films on the as-cast and FSPed NAB, because Cl was enriched there, as indicated by the EPMA results in Figure 8.

The above results demonstrated that the corrosion product films formed on the as-cast and FSPed NAB were similar in composition. However, the following factor attributed to the superior protectiveness of the film on the FSPed NAB. During the heating process of FSP, part of the α and κ phases with abundant Fe, Ni and Al contents in the as-cast NAB were transformed into the β phases.[7] In the following rapid cooling process, there was no sufficient time for the κ phases to precipitate completely; hence more Fe, Ni and Al were retained in α and β'. For the FSPed NAB, more Fe, Ni and Al participated in the formation of the corrosion product film rather than retained in the uncorroded phases. Namely more Fe and Ni incorporated into the lattice of $Cu_2O$ and more $Al_2O_3$ was formed. Therefore, the corrosion product film formed on the FSPed NAB was more protective.

As discussed above, the interfaces between the uncorroded phases and their surrounding corrosion products allowed the chloride ions into the corrosion product

film. The chloride ions reacted with $Cu_2O$ and $Cu_2(OH)_3Cl$ was then formed. This could explain why $Cu_2(OH)_3Cl$ was mainly distributed over the lamellar α + $\kappa_{III}$ phases for the as-cast NAB, and over the β' phases for the FSPed NAB. For the as-cast NAB, the uncorroded κ phases in the corrosion product film were much larger in size or continuous in structure, resulting in more susceptible interfaces between them and their surrounding corrosion products; therefore, $Cu_2(OH)_3Cl$ was found in much larger amount in the corrosion product film formed on the as-cast NAB.

**Stability of the corrosion product films in the flowing condition**

Figure 9 shows the Nyquist and Bode plots of the filmed as-cast and FSPed NAB after different erosion periods in a flowing medium, i.e., a 3.5 wt.% NaCl solution containing 1 wt.% silica sand at a velocity of 4 m/s. At 0 h, the impedance |Z| of the filmed FSPed NAB is about one magnitude larger than that of the filmed as-cast NAB, indicating that the film on the FSPed NAB is more protective. This finding is consistent with our previous study.[14] For the as-cast and FSPed NAB, the semi-diameter of the capacitive reactance arc in the Nyquist plot decreases and an inductive arc appears at the lower frequency range with the increasing erosion time, as shown in Figure 9(a). Correspondingly, the film impedance |Z| also decreases; moreover, the time constant at the low frequency which is attributed to the barrier property of the corrosion product film moves to the higher frequency side and gradually disappears with the increasing erosion time, as indicated in Figures 9(b) and (c). These findings indicate that the films on the as-cast and FSPed NAB are gradually damaged. In the first 2 hours, the film impedance |Z| of the FSPed NAB is larger than

that of the as-cast NAB, indicating that the film on the FSPed NAB exhibits better stability in the flowing condition. At 3 h, the Nyquist plots of the as-cast and FSPed NAB are very close to each other. This demonstrates that the corrosion product films on the as-cast and FSPed NAB are totally damaged.

In the flowing condition, if a second phase (solid particle, gas bubble, etc.) in the main fluid impinged directly on the metal surface, the repeated dynamic forces would result in the initiation and propagation of fatigue, such as cracks, inside the corrosion products on the metal surface.[28] Moreover, corrosion product films exhibited brittle erosion characteristics, the erosion of the corrosion product films occurred when the solid particles had a sufficiently high velocity component normal to the metal surface.[28] In this study, the flow condition was in a turbulent state and the solid particles in the flowing medium impinged on the filmed as-cast and FSPed NAB with a sufficiently high normal component of the velocity. A possible film damage mechanism was raised here, as schematically indicated in Figure 10. The outer layers of the corrosion product films were discontinuously distributed and hardly protective, they were rapidly removed in the flowing medium. As stated above, undissloved phases were found in the corrosion product films on the as-cast and FSPed NAB. Under the impingement of the flowing medium, cracks probably formed and propagated along the interfaces between the uncorroded phases and their surrounding corrosion products preferentially. For the as-cast NAB, the uncorroded phases inside the corrosion product film were large in size, continuous in the structure, and even partly in the film and partly in the substrate, as demonstrated in Figure 10(a).

Therefore, cracks initiated and extended along the depth easily; moreover, the corrosive medium was allowed in, as indicated in Figure 10(b). With the increasing erosion time, cracks extended to the substrate as shown in Figure 10(c), resulting in the complete failure of the film. For the FSPed NAB, cracks also preferentially formed and extended along the susceptible interfaces between these phases and their surrounding corrosion products under the impingement of the flowing medium, as shown in Figure 10(e). However, the uncorroded phases were much smaller in size and dispersedly distributed, as demonstrated in Figure 10(d). Therefore, it was hard for these cracks to join together and extend further along the depth. With the increasing erosion time, the film was gradually thinned and the retained corrosion product film was still protective, as shown in Figure 10(f). Therefore, the corrosion product film on the FSPed NAB was more resistive in the flowing condition than that on the as-cast NAB.

## CONCLUSIONS

1. Greatly refined microstructures were obtained in an as-cast NAB via FSP.
2. The mass loss of the FSPed NAB was much smaller than that of the as-cast NAB after immersion in a stagnant 3.5 wt.% NaCl solution. Corrosion mainly occurred at the lamellar α + $\kappa_{III}$ phases for the as-cast NAB and at the β' phases for the FSPed NAB. Much deeper corrosion pits were found in the as-cast NAB.
3. Uncorroded phases were found in the corrosion product films on the the as-cast and FSPed NAB. The interfaces between these phases and their surrounding

corrosion products allowed the chloride ions in and reduced the film protectiveness. For the as-cast NAB, the interfaces were continuous because the uncorroded phases were large in size or continuous in structure. For the FSPed NAB, the interfaces were discontinuous because the uncorroded phases were small in size and had a dispersed distribution. This was the main reason why the film formed on the as-cast NAB was less protective than that on the FSPed NAB.

4. For the as-cast and FSPed NAB, the corrosion product films consisted of two layers. The outer later was mainly discontinuous $Cu_2(OH)_3Cl$ and the inner layer was $Al_2O_3$ and $Cu_2O$ with the incorporation of Fe and Ni.

5. In the flowing condition, the corrosion product film on the FSPed NAB presented superior protectiveness. The film on the as-cast NAB was damaged by formation and expansion of the cracks; whereas the film on the FSPed NAB was damaged by thinning.

## ACKNOWLEDGEMENT

This work was supported by the National Natural Science Foundation of China (No. 51131008).

## REFERENCES

1. E.A. Culpan, G. Rose, Br. Corros. J. 14 (1979): p.160.

2. A. Al–Hashem, P.G. Caceres, W.T. Riad, H.M. Shalaby, Corrosion 51 (1995): p.331.

3. J. A. Wharton, R. C. Barik, G. Kear, R. J. K. Wood, K. R. Stokes, F. C. Walsh, Corros. Sci. 47 (2005): p.3336.

4. A. Schüssler, H.E. Exner, Corros. Sci. 34 (1993): p.1793.

5. A.H. Tuthill, Mater. Performance 26 (1987): p.12.

6. J.P. Ault, Corrosion 95, Paper No. 281, NACE International, Houston, Texas, 1995.

7. D.R. Ni, P. Xue, D. Wang, B.L. Xiao, Z.Y. Ma, Mater. Sci. Eng. A 524 (2009): p.119.

8. W.M. Thomas, E.D. Nicholas, J.C. Needham, M.G. Murch, P. Temple–Smith, C.J. Dawes, G.B. Patent Application No. 9125978.8, 1991.

9. R.S. Mishra, Z.Y. Ma, Mater. Sci. Eng. R 50 (2005): p.1.

10. M. Atapour, A. Pilchak, G.S. Frankel, J.C. Williams, Corros. Sci. 52 (2010): p.3062.

11. M.L. Santella, T. Engstrom, D. Storjohann, T. –Y. Pan, Scripta Mater. 53 (2005): p.201.

12. D.R. Ni, B.L. Xiao, Z.Y. Ma, Y.X. Qiao, Y.G. Zheng, Corros. Sci. 52 (2010): p.1610.

13. K. Oh–ishi, T.R. McNelley, Metall. Mater. Trans. A 36A (2005): p.1575.

14. Q.N. Song, Y.G. Zheng, S.L. Jiang, D.R. Ni, Z.Y. Ma, Corrosion 69 (2013): p.1111.

15. Q.N. Song, Y.G. Zheng, D.R. Ni, Z.Y. Ma, Corrosion 70 (2014): p.261.

16. F. Hasan, A. Jahanafrooz, G.W. Lorimer, and N. Ridley, Metall. Trans. A 13A (1982): p.1337.

17. S. Neodo, D. Carugo, J.A. Wharton, K.R. Stokes, J. Electroanal. Chem. 695 (2013): p.38.

18. G.W. Lorimer, F. Hasan, J. Iqbal, N. Ridley, Br. Corros. J. 21 (1986): p.244.

19. B.G. Ateya, E.A. Ashour, S.M. Sayed, J. Electrochem. Soc. 141(1994): p.71.

20. C. Kato, B.G. Ateya, J.E. Castle, H.W. Pickering, J. Electrochem. Soc. 127 (1980): p.1897.

21. F. Mansfeld, G. Liu, H. Xiao, C.H. Tsai, B.J. Little, Corros. Sci. 36 (1994): p.2063.

22. J.M. Popplewell, R.J. Hart, J.A. Ford, Corros. Sci. 13 (1973): p.295.

23. R. F. North, M.J. Pryor, Corros. Sci. 10 (1970): p.297.

24. I. Milošev, M. Metikoš–Hukovic, Electrochim. Acta 42(1997): p.1537.

25. W.A. Badawy, F.M. Al–Kharafi, A.S. El–Azab, Corros. Sci. 41 (1999): p.709.

26. H. Nady, N.H. Helal, M.M. El–Rabiee, W.A. Badawy, Mater. Chem. Phys. 134 (2012): p.945.

27. J.C. Scully, The Fundamentals of Corrosion, Pergamon Press, Oxford, 1990.

28. T. Sydberger, Br. Corr. J. 22 (1987): p. 83.

# FIGURES

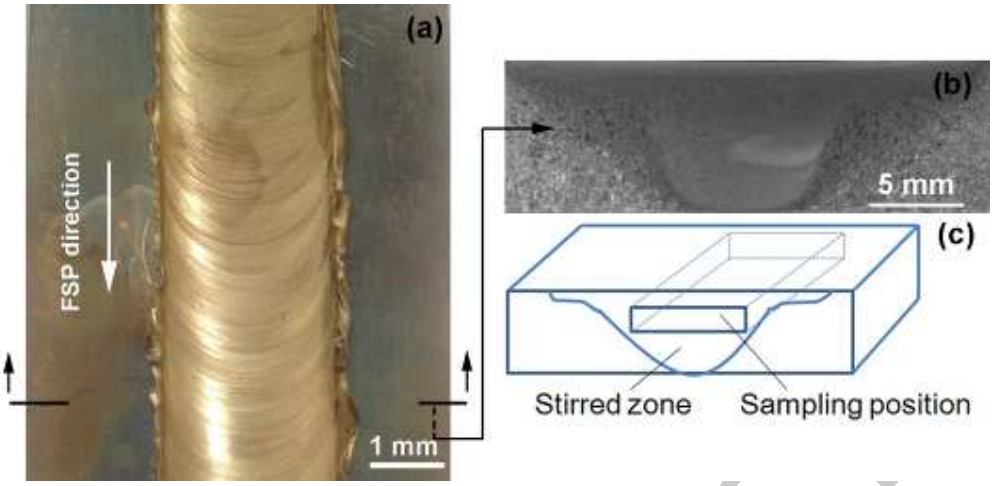


FIGURE 1. *(a) Top view, (b) stirred zone and (c) schematic diagram for the sampling position of the FSPed NAB.*

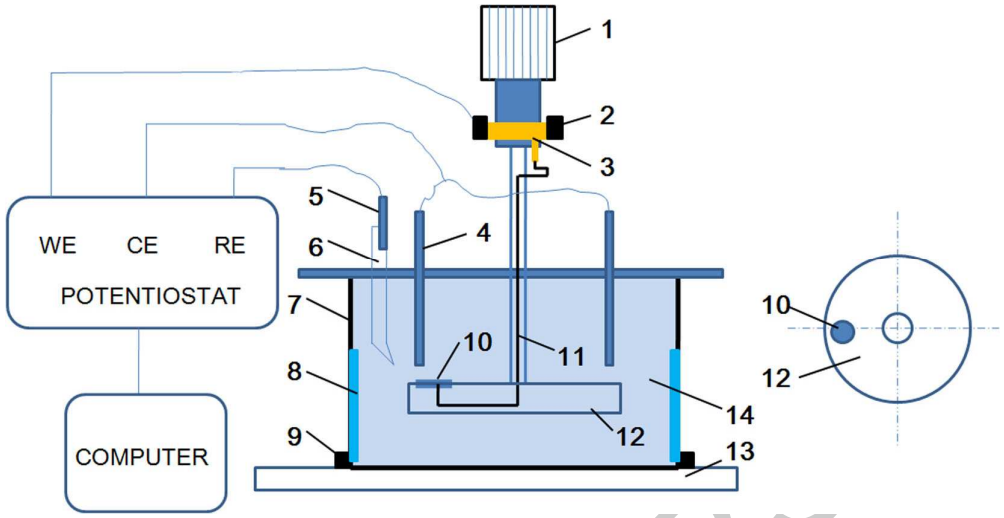


FIGURE 2. *Schematic diagram of a modified rotating disc rig. 1. Rotator, 2. Graphite brush, 3. Copper ring and connector, 4. Graphite rod, 5. Saturated calomel electrode (SCE), 6. Salt bridge, 7. Container, 8. Baffle, 9. Fastener, 10. Working electrode, 11. Wire, 12. Rotating disc, 13. Support platform, 14. Flowing medium.*

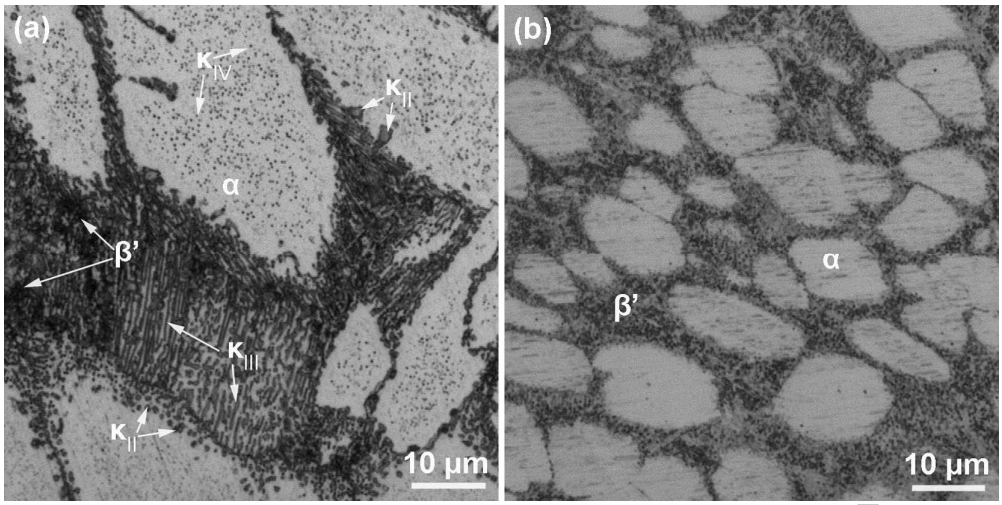


FIGURE 3. *Optical microstructures of the (a) as-cast NAB and (b) center in the stirred zone of the FSPed NAB.*

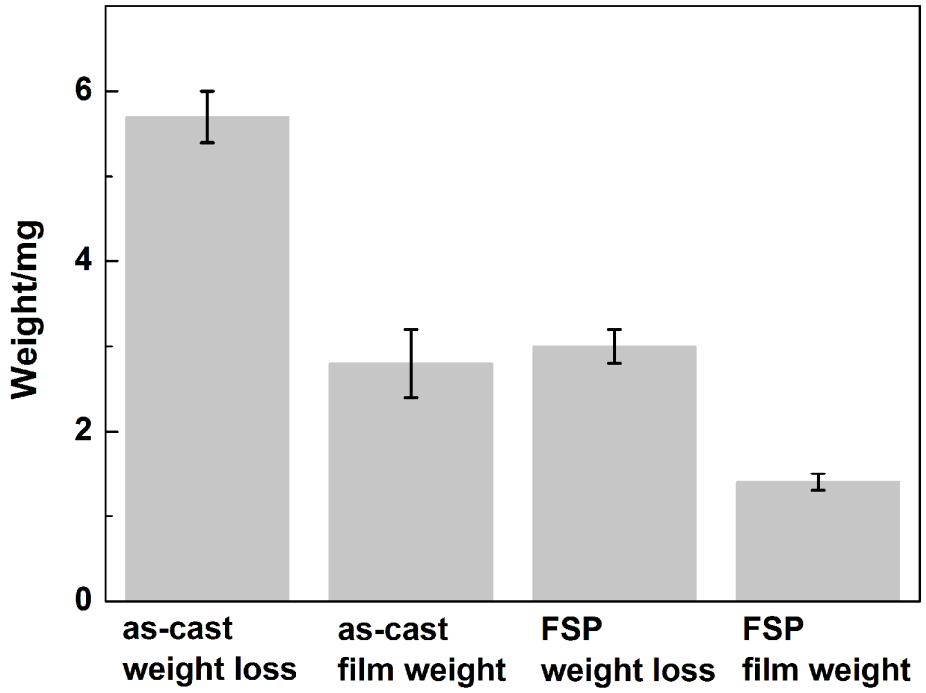


FIGURE 4. *Weight loss and weight of the corrosion product film for the as-cast and FSPed NAB after immersion in a 3.5 wt.% NaCl solution for 60 days.*

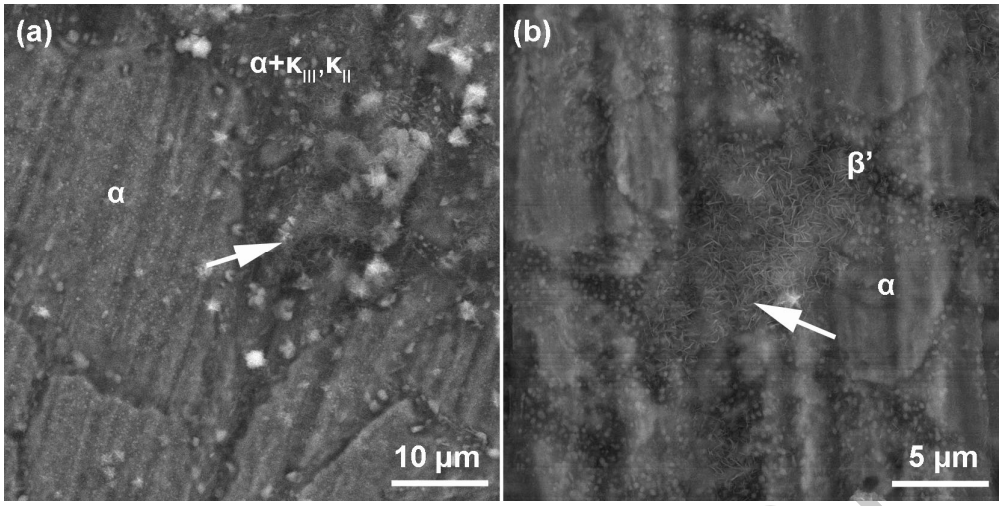


FIGURE 5. *Surface morphologies of the (a) as-cast and (b) FSPed NAB after immersion in a 3.5 wt.% NaCl solution for 60 days.*

1

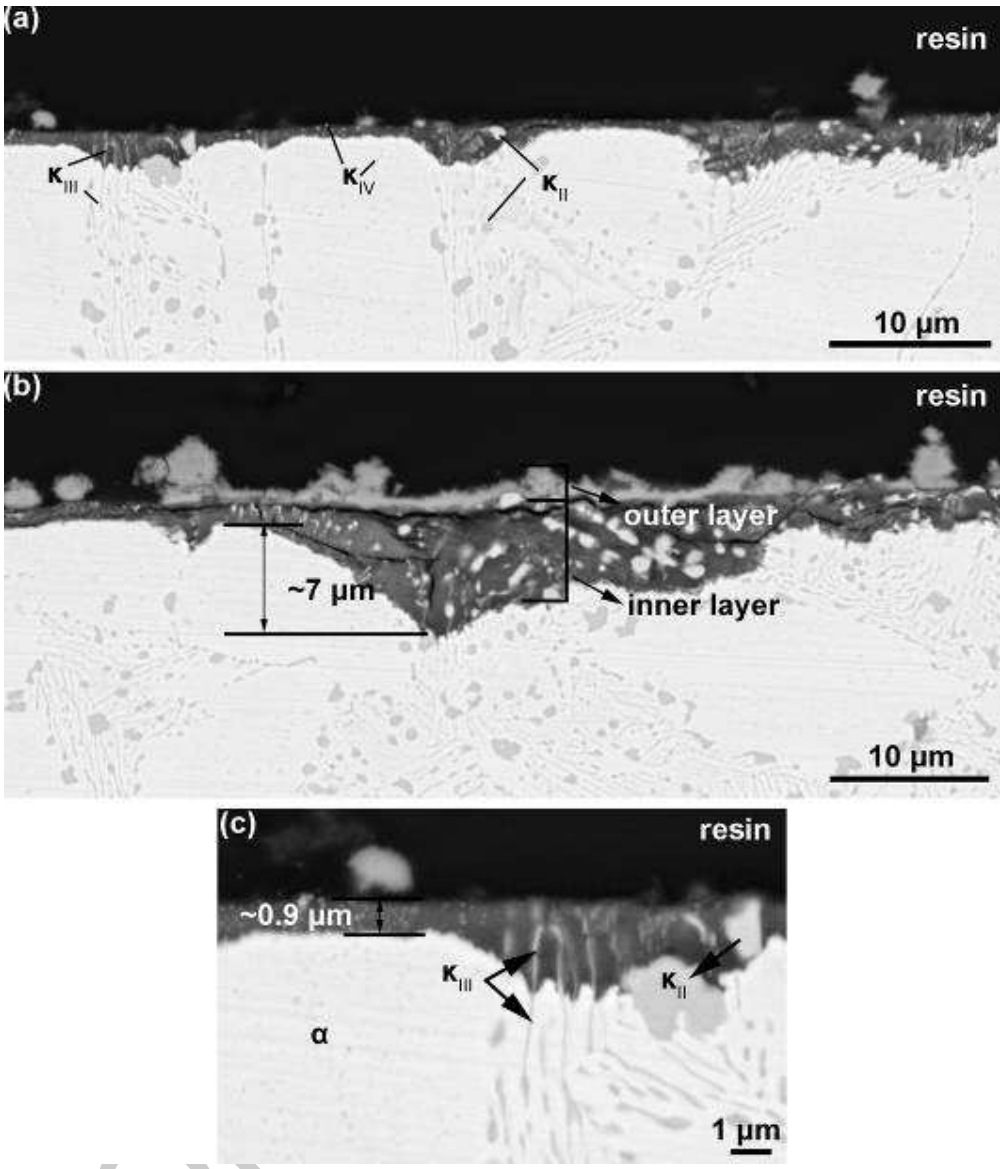
(a)
resin
$K_{III}$
$K_{IV}$
$K_{II}$
10 µm
(b)
resin
outer layer
~7 µm
inner layer
10 µm
(c)
resin
~0.9 µm
$K_{III}$
$K_{II}$
α
1 µm

2

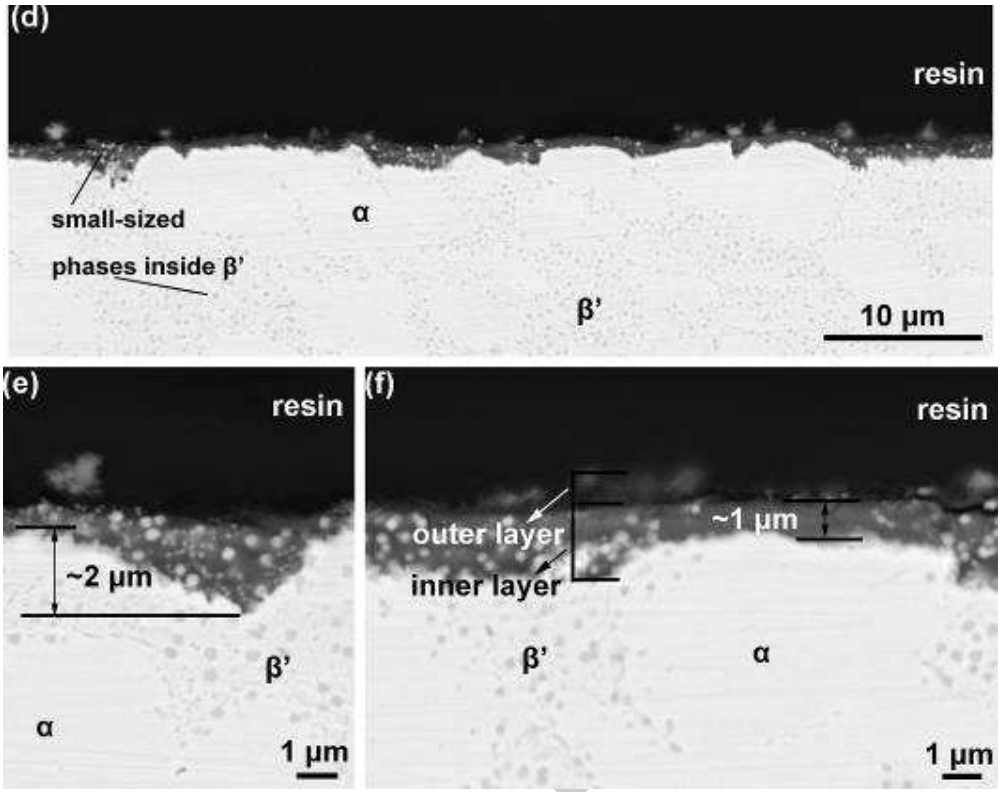


FIGURE 6. *Cross section BSE images of the (a–c) as-cast and (d–f) FSPed NAB after immersion in a 3.5 wt.% NaCl solution for 60 days.*

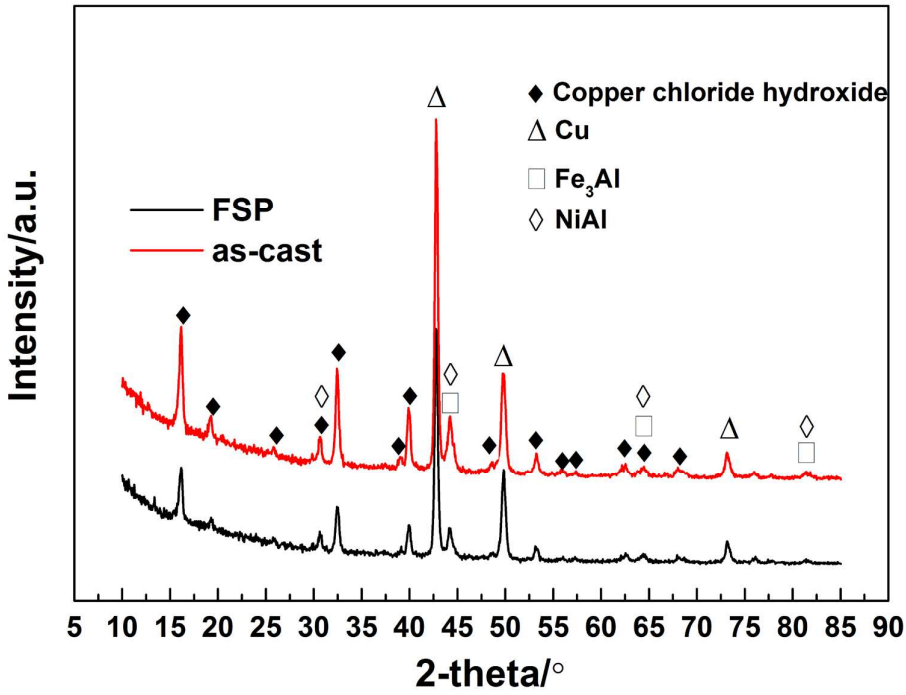


FIGURE 7. *XRD patterns of the corrosion product films on the as-cast and FSPed NAB after immersion in a 3.5 wt.% NaCl solution for 60 days.*

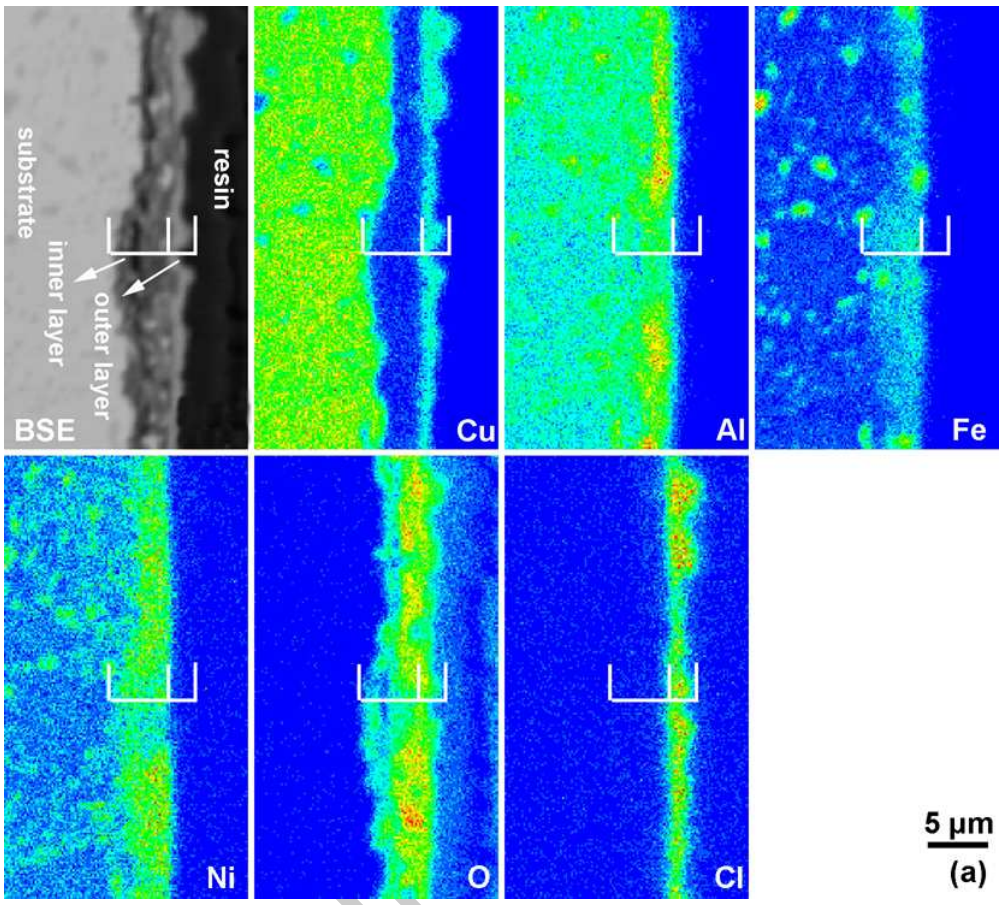
substrate
resin
inner layer
outer layer
BSE
Cu
Al
Fe
Ni
O
Cl
5 µm
(a)

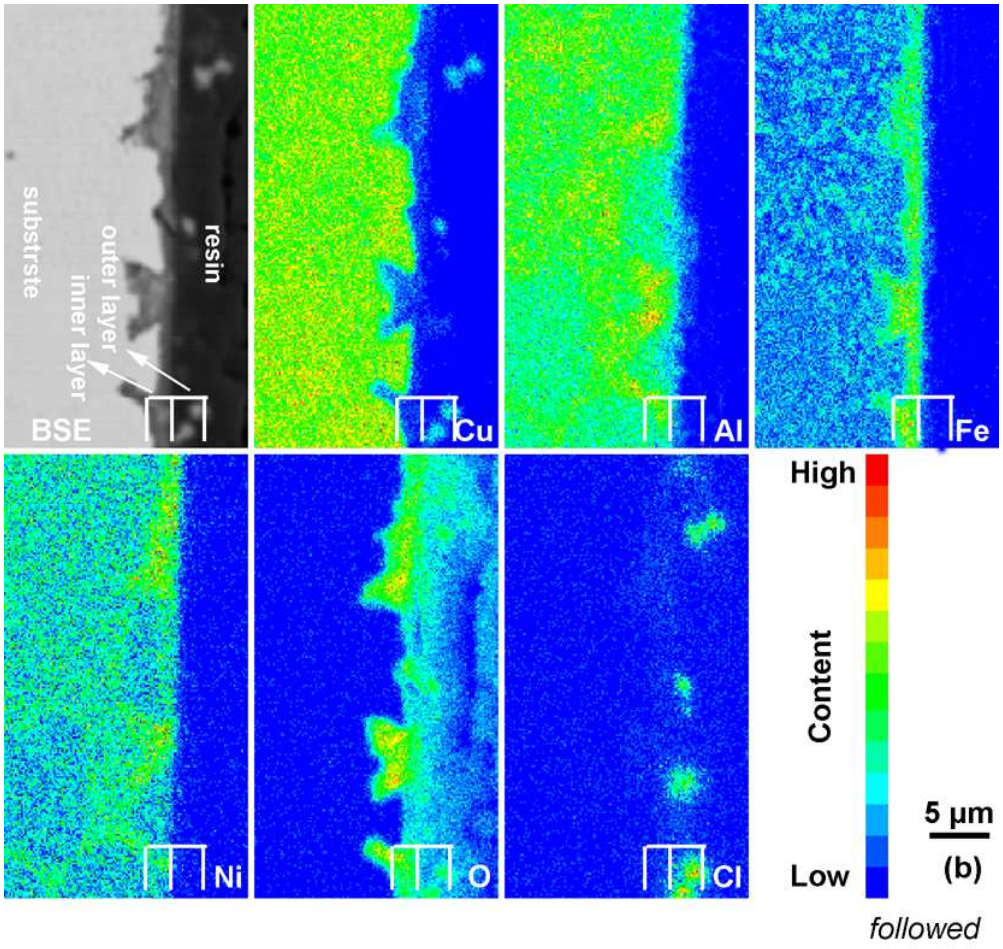


FIGURE 8. *Element mapping of the corrosion product films in the cross section for the (a) as-cast and (b) FSPed NAB after immersion in a 3.5 wt.% NaCl solution for 60 days.*

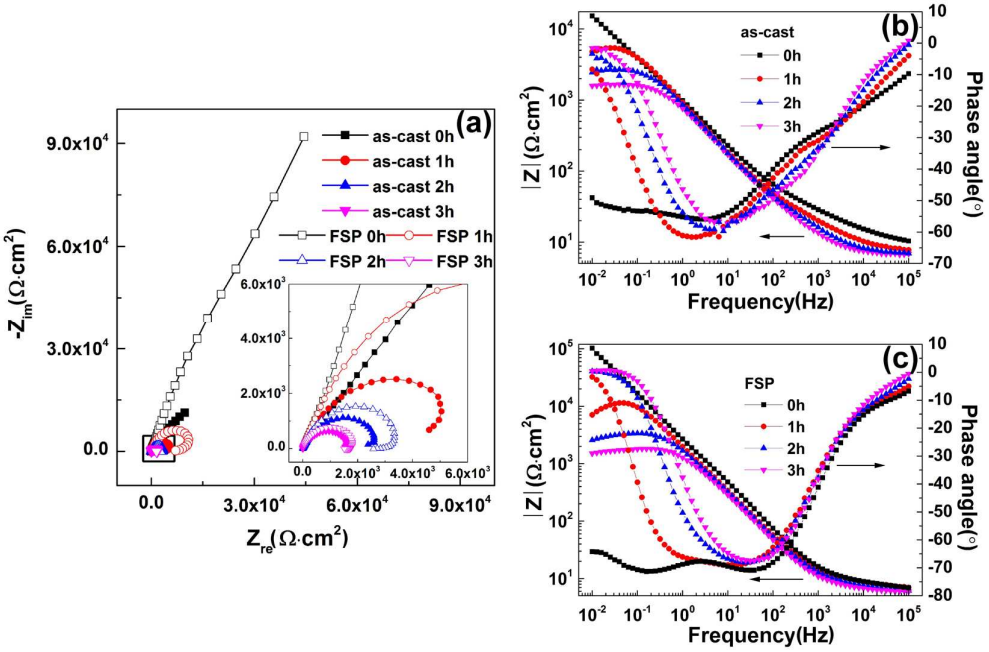


FIGURE 9. *(a) Nyquist and Bode plots of the filmed (b) as-cast and (c) FSPed NAB (after immersion in a stagnant 3.5 wt.% NaCl solution for 60 days ) with the erosion time in a flowing 3.5 wt.% NaCl solution containing 1 wt.% silica sand at a velocity of 4 m/s.*

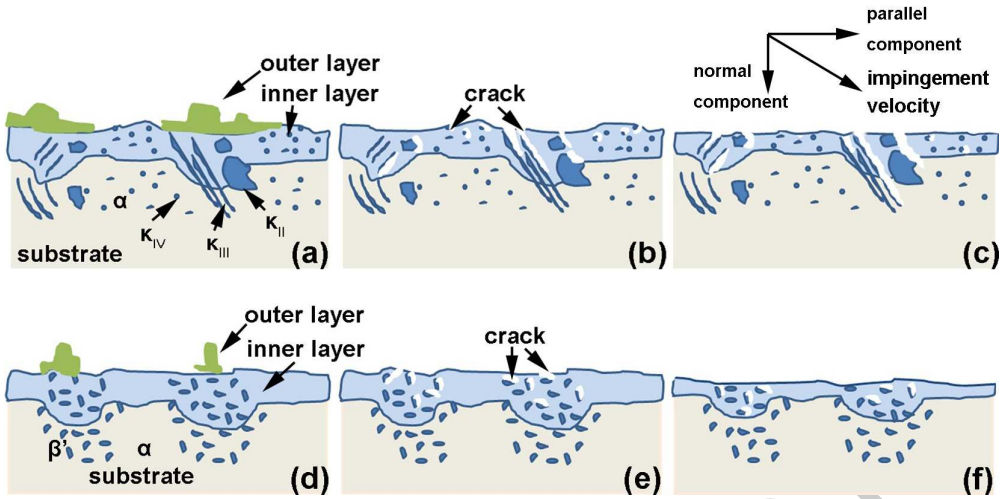


FIGURE 10. *Schematic diagram for the damage process of the corrosion product films on the as-cast and FSPed NAB in a flowing 3.5 wt.% NaCl solution containing 1 wt.% silica sand. As cast NAB: (a) before erosion, (b) crack formation,(c) crack extending into the substrate; FSPed NAB: (d) before erosion, (e) crack formation, (f) thinning of the corrosion product film.*